1
2
3
4
5
6
7
8
9
10
11
12
13
14
15
16
17
18
19
20
21
22
23
24
25
26
27
28
29
30
31
32
33
34
35
36
37
38
39
40
41
42
43
44
45
46
47
48
49
50
51
52
53
54
55
56
57
58
59
60

Critical Size for Carrier Delocalization in Doped Silicon Nanocrystals: A Study by Ultrafast Spectroscopy

Rens Limpens[#1], Hiroshi Sugimoto[2], Nathan R. Neale[1] & Minoru Fujii[2]

[1]Chemistry and Nanoscience Center, National Renewable Energy Laboratory, 15013 Denver West Parkway, Golden, CO 80401, USA.

[2]Department of Electrical and Electronic Engineering, Kobe University, Rokkodai, Nada, Kobe 657-8501, Japan.

[#]Corresponding author: Rens Limpens. E-mail: rens.limpens@nrel.gov.

Abstract

We present a comprehensive ultrafast spectroscopy-based study on the delocalization of doping-induced carriers in Si nanocrystals (NCs). To this end we prepare thin films of differently-sized doped Si NCs and vary the doping configurations from singly P and B doping to simultaneously P and B co-doping. We show that the NC size orchestrates the level of delocalization of the doping-induced carriers. This can be understood in light of (1) the quantum confinement effect and (2) unscreened Coulomb interactions by moving further into the nanoscale. Both contributions affect the activation energy (ΔE) that is required to create free majority carriers. By varying the NC size in combination with the doping configuration we tune ΔE and control the delocalization of the doping-induced carriers. Most importantly, we show that there is a critical NC diameter of $D_{critical}$≈6 nm that describes the transition from a localized to a free-carrier regime. In particular, our results show that optical bandgaps of ≈0.95 eV (optimal for carrier multiplication-facilitated solar cell power conversion) can be achieved in P-B co-doped Si NCs with $D_{NC} < D_{critical}$. These results indicate that the practical photovoltaic feasibility of co-doped Si NCs is not limited by the presence of some remaining free carriers in uncompensated NCs.

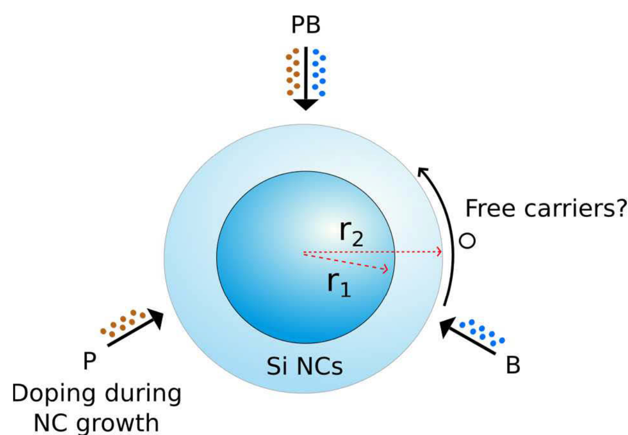

Keywords: silicon nanoparticles, substitutional doping, ultrafast spectroscopy, Auger interactions, free carriers, photovoltaics.

Introduction

Siilicon nanocrystals (Si NCs) are under intense investigation for their promise in next-generation solar cells. In one concept, these non-toxic NCs would make use of efficient carrier multiplication[1–3] to prevent thermalization losses and potentially beat the Shockley-Queisser limit.[4,5] Although serious advances have been made in metal chalcogenide and lead halide perovskite NC-based solar cells,[6–9] advanced photovoltaic (PV) concepts based on Si NCs have

Pursuant to the DOE Public Access Plan, this document represents the authors' peer-reviewed, accepted manuscript. The published version of the article is available from the relevant publisher.

yet to be achieved. For Si NCs to become viable in advanced PV concepts, the two primary challenges that need to be overcome are low inter-NC electrical conductivities[10] and the large quantum-confined bandgap of Si NCs (1.2–1.8 eV) that is far from the optimal power conversion bandgap of ~0.9 eV.[5] Recently, a possible game changer arose in the form of co-doped Si NCs[11–13] that are simultaneously doped with both phosphorous (P) and boron (B) doping species. With their surface chemistry modifications[13] and optimal carrier multiplication features[14] they might tackle both of these problems at the same time. In parallel to these co-doped structures, singly doped (n- or p-type) Si NCs have shown their value for the optoelectronic industry as well and could be employed as e.g., fluorescent markers for biosensing purposes[15,16] or even photodetectors.[17]

While the application potential of doped Si NCs is enormous (especially considering the tremendous Si-based infrastructure that is already installed) it is striking to realize that the photo-physics in these systems are barely understood. Only recently, the energies of the donor and acceptor states in Si NCs and its size dependence were experimentally determined for co-doped Si NCs.[18,19] This information is still missing in singly doped Si NCs. In addition, factors that determine the density of free carriers, e.g., a kind of dopant atom, degree of compensation by co-doping, surface passivation, dielectric environment of NCs, etc., have never been comprehensively discussed. Lastly, it is not clear to what extent the photo-excited carrier lifetimes are affected by the doping process and, if so, what causes this. Several reports claim to observe nonradiative trion recombination as a result of Coulomb interactions between the photo-excited carriers and the doping-introduced free carriers.[20–22] We showed that this is true for large diameter (D_{NC}) > 7 nm P-doped Si NCs, and defined – by means of ultrafast spectroscopy – the negative trion recombination lifetime to be ≈9 ns.[23] Other reports have claimed that doping-induced defect states, most likely arising from interstitially-positioned and surface-located doping atoms, actually dominate the carrier dynamics and as such limit their practical feasibility.[24–27] We also showed that this holds for relatively small P and B co-doped Si NCs (D_{NC} < 6 nm) embedded in SiO_2. As previously argued by ourselves[28] and others,[29,30] this apparent discrepancy could possibly be explained by a NC size effect where the activation energy of the doping-induced carriers, ΔE, defines their mobility. Above a certain ΔE, carriers are free, whereas below the threshold ΔE, carriers are localized on their original dopant atom. However, without a comprehensive discussion and extensive experimental results, the ability to assess the practical limitations and envision device structures to optimize doped Si NCs for future electronics relies solely on theoretical works.[30]

In this experimental work we aim to resolve this controversy by presenting a complete picture of the nature of the dopant-induced carriers and the forthcoming photophysics in Si NCs. We make use of ultrafast induced absorption (IA) spectroscopy to examine a series of Si NC samples with systematically varied NC size and dopant configuration (type and concentration). These experiments provide a quantification of the critical NC size ($D_{critical}$) at which delocalization of the doping-induced carriers occurs.

Materials and Methods

Co-sputtered NC films

Pursuant to the DOE Public Access Plan, this document represents the authors' peer-reviewed, accepted manuscript. The published version of the article is available from the relevant publisher.

1 2 3 4 5 6 7 8 9 10 11 12 13 14 15 16 17 18 19 20 21 22 23 24 25 26 27 28 29 30 31 32 33 34 35 36 37 38 39 40 41 42 43 44 45 46 47 48 49 50 51 52 53 54 55 56 57 58 59 60

Briefly, Si and SiO_2 along with B_2O_3 and/or P_2O_5 for doped samples are sputter-deposited on silica substrates. The composition of a film is changed by varying the area ratio between the source materials. The thicknesses of as deposited films are estimated to be 1.5 μm. Thermal annealing in N_2 atmosphere facilitates Si diffusion and NC growth, and varying the annealing temperature results in samples with different NC diameters. The presence of P and/or B results in these elements becoming incorporated during the NC growth. Further details can be found in Ref.[[31]].

Photoluminescence

PL spectra were measured using a spectrofluorometer (Fluorolog-3, HORIBA Jovin Yvon) equipped with a photomultiplier (500–850 nm) and an InGaAs photodiode (800–1300 nm) as detectors. The PL spectra obtained by the two different detectors are merged after correcting the sensitivity. The correction factors were obtained by measuring the reference spectrum of a standard halogen lamp. As excitation source we used a 365 nm monochromatized Xe lamp.

Induced absorption

Induced absorption (IA) experiments were conducted on a pump−probe setup, using a femtosecond transient absorption spectrometer (Helios, Ultrafast Systems) with a 4 W Ti:sapphire amplifier (Libra, Coherent) laser source, operating at 1 kHz and 100 fs pulse width. All IA experiments have been conducted with λ_{pump} =500 nm and λ_{probe} =1200 nm. This infra-red (IR) probe is typical for IA spectroscopy on Si NCs, since the indirect bandgap prohibits efficient interband transitions.[3] As a result of our IR intraband probing beam we observe an induced absorption effect upon the creation of pump-created electron-hole (e^--h^+) pairs. For all probing wavelengths along the investigated probing range (1000-1400 nm) we observe identical carrier dynamics (Figure S10) for all samples, indicating the absence of a resonant probing effect of the doped states. This is expected due to their relatively low density of states compared to the electronic structure of the Si NCs. Furthermore, pump fluences of around 0.6 mJ/cm^2 have been used to excite the single-exciton excitation regime, providing Nabs values <<1 – See Supporting Information for more details.

Results & Discussion

(Doped) Si NC systems

Type of Si NCs	Annealing temperature (°C)	Estimated P and B concentration (at.%)
Intrinsic	1050, 1100, 1150, 1200	-
Singly B-doped	1050, 1100, 1150, 1200	B: 0.9
Singly P-doped	1050, 1100, 1150, 1200	P: 0.6
Low concentration P-B co-doped (LPB)	1050, 1100, 1150, 1200	P: 0.3; B: 0.8
High concentration P-B co-doped (HPB)	1050, 1100, 1150, 1200	P: 0.6; B: 0.9

Table 1. Sample characteristics. Estimated P and B concentrations reflect the average concentration in the sputtered films.

The list of samples is summarized in Table 1. All samples are prepared by the same co-sputtering method (Materials and Methods). We study four doping-types: intrinsic, singly P-

Pursuant to the DOE Public Access Plan, this document represents the authors' peer-reviewed, accepted manuscript. The published version of the article is available from the relevant publisher.

doped, singly B-doped and P-B co-doped Si nanostructures. Two doping concentrations of these co-doped structures have been produced, referred to as "low" (LPB) and "high" (HPB) reflecting the P and B concentrations in sputtered films of 0.3 P and 0.8 B at.% for LPB and 0.6 P and 0.9 B at.% for HPB. The singly doped systems are only produced in the high doping concentration variant i.e., 0.6 at.% for P and 0.9 at.% for B. These doping concentrations are obtained from integral intensities of x-ray photoelectron spectroscopy, by taking into account the photo-ionization cross-sections of each element (Figure S1). Note that for the singly P- and B-doping types, all substitutional doping sites will contribute to the number of doping-induced carriers. For the P-B co-doped systems, the carrier concentration relies on incomplete charge compensation, which lowers the carrier concentration tremendously in comparison to the singly-doped NCs.

Characterization by photoluminescence spectroscopy

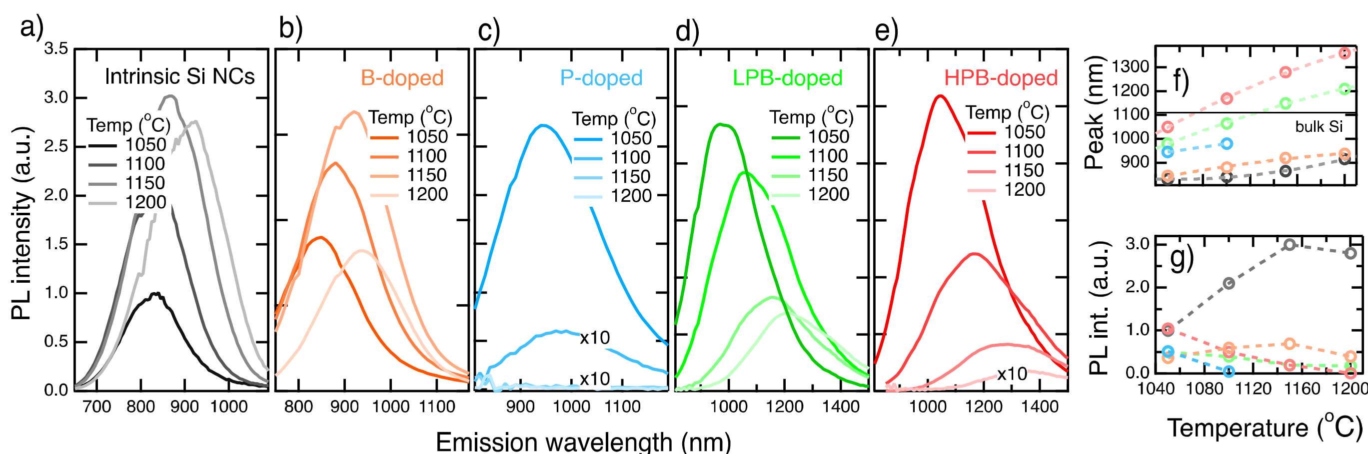

Figure 1. PL of the optically active Si NC ensembles, at four different annealing temperatures ranging from 1050 to 1200 °C. Photoexcitation has been performed at $\lambda_{exc} = 365$ nm. PL spectra of the intrinsic Si NCs in black (a), B-doped in orange (b), P-doped in blue (c), LPB co-doped Si NCs in green (d) and HPB co-doped Si NCs in red (e). PL Peak positions (f) and integrated relative PL intensities (g) of all spectra as a function of the annealing temperature.

Figure 1 displays the optical characterization of our emissive NC ensembles by photoluminescence (PL) spectroscopy. Panels (a-e) show all PL spectra, (f) and (g) their respective PL peak position and integrated relative PL intensities. Note that the absorbance at λ_{exc}= 365 nm is similar for all NC ensembles (Figure S2). We can therefore treat the relative PL intensities as their relative PL quantum yield values. The intrinsic Si NCs (Figure 1a) exhibit emission spectra peaking around ≈810-910 nm, red-shifting with the annealing temperature, consistent with relaxing quantum confinement due to temperature-induced NC growth.[32] This corresponds to a NC size variation from 3 to 4 nm – size-estimations are derived from their PL spectra following Ref.[33] We cannot simply make size-estimations for the doped NCs based on their PL characteristics, further evaluation regarding their sizes follows later on. Interestingly, the incorporation of singly-doping does not necessarily suppress radiative recombination by free carrier-driven nonradiative trion recombinations. This is illustrated by the emission from all

Pursuant to the DOE Public Access Plan, this document represents the authors' peer-reviewed, accepted manuscript. The published version of the article is available from the relevant publisher.

of the singly B-doped (Figure 1b) and the lowest annealing temperatures of the singly P-doped systems (Figure 1c) as well, red-shifting with the annealing temperature. This result touches on a major aspect of this work and will be discussed below. Overall, the B-doped NC emission energy is very similar to the intrinsic NC emission, whereas the P-doped NCs show significant red-shifted emission (≈950-1000 nm) in relation to the intrinsic NCs. Both the LPB and HPB P-B co-doped NC systems (Figure 1d,e) exhibit PL at significantly longer wavelengths (≈1000-1200 nm for LPB and ≈1050-1350 nm for HPB) in comparison to their intrinsic – or even singly doped cousins. These red-shifted emission spectra are indicative of the below bulk Si bandgap (illustrated by the black line in Figure 1f) donor-acceptor transitions characteristic of these samples.[18,34] Furthermore, the emission wavelength of the HPB NCs is longer than that of the LPB sample, in line with the higher doping concentration that red-shifts the lowest optical transition.[35]

Ultrafast carrier dynamics by induced absorption spectroscopy

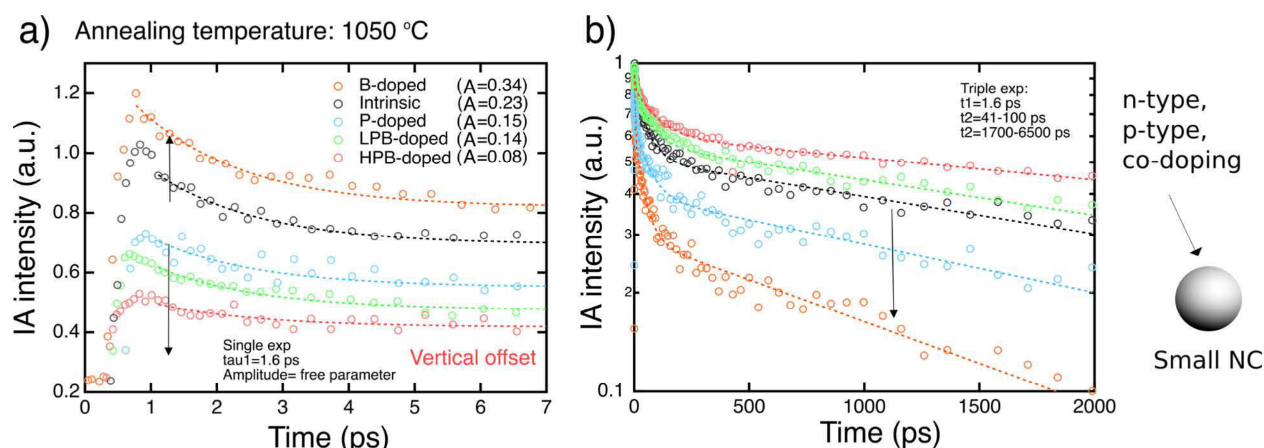

Figure 2. IA transients for all types of NC ensembles at an annealing temperature of T=1050 ^{o}C. a) Traces on <7 ps time-scales. Same color scheme is used as in Figure 1. A vertical offset has been applied for clarity. The dashed lines represent single exponential fits. b) The same traces plotted on a longer time-scale (up to 2 ns). These traces are ordered based on their respective average decay rate. The dashed lines are triple exponential fits preformed according to the fitting method of Figure S5.

Figure 2 displays IA traces of all types of NC systems at their lowest annealing temperature (T_{an}=1050 ^{o}C), resulting in the smallest NC sizes of this study. Experimental details are given in the Methods. Unless mentioned otherwise, all traces are taken in the single-exciton excitation power regime, in which at most a single photo-excited electron-hole (e^--h^+) pair is created per NC. Derivation of this single-exciton excitation power regime is performed in Figure S3. The doping-induced carriers in these small NCs are expected to be localized to their original dopant atom, due to their large activation energies ΔE.[19,30] As such, Coulomb interactions between photo-excited e^--h^+ pairs and these localized carriers will be negligible[28] (as will be confirmed later on in this work), and the decaying IA traces should directly reflect the NC quality. In Figure 2a we focus on the initial fast decay (fitted with a single exponential lifetime of =1.6 ps). This

Pursuant to the DOE Public Access Plan, this document represents the authors' peer-reviewed, accepted manuscript. The published version of the article is available from the relevant publisher.

1
2
3
4
5
6
7
8
9
10
11
12
13
14
15
16
17
18
19
20
21
22
23
24
25
26
27
28
29
30
31
32
33
34
35
36
37
38
39
40
41
42
43
44
45
46
47
48
49
50
51
52
53
54
55
56
57
58
59
60

recombination channel has previously been assigned to oxygen-initiated surface defect states.[23,28,36,37] We quantify the magnitude of this ultrafast carrier loss by the amplitude A of the single exponential fit. By applying a vertical offset, we order the traces according this amplitude-value and discuss the introduced doping-effect. Whereas singly P-doping (A=0.15) and both P-B co-doping concentrations (A=0.14 and A=0.08 for LPB and HPB, respectively) decrease the initial carrier loss (i.e., improve the surface passivation cf. intrinsic Si NCs, with A=0.23), the IA trace of the B-doped NCs (A=0.34) indicates a lower level of surface passivation. To this end we note that doping has been shown to improve the surface quality for P-doped,[38] B-doped[39] and P-B co-doped NC structures,[28] but only for certain concentrations.[20,39] Specifically for B-doped NCs, impurity concentrations for surface passivation optimization are fairly low (> $2.5x10^{18}$ cm^{-3}), as established by Putheen et al.[39]. By geometrical arguments this resembles <<1 impurities in a Si NC with D_{NC}=3 nm. Recent atom probe tomography work[40] on samples similar to those studied here shows that in ensembles of singly B-doped NCs >90% of the NCs contain B atoms. We therefore argue that the fast dynamics for the B-doped NCs likely results from a high concentration of B atoms at the NC surface, well in excess of the optimal passivation value (i.e., >>$2.5x10^{18}$ cm^{-3}). In Figure S4 we show the generalization of this passivation effect for all annealing temperatures. Also, the passivation effect could be restricted to our type of samples: SiO_2-embedded NCs not treated by a forming gas passivation step. We do note that even after forming gas annealing, luminescence quantum yields of Si NCs in silica or silicate matrices are below 35%[32] and thus there remains a significant number of defects which could potentially still be passivated by our doping atoms, likely resulting in the same effect.

Figure 2b presents the carrier dynamics on a longer time-scale (up to 2 ns). We fit the complete traces with triple exponential models (details of the fitting method can be found in the Supporting Information – Figure S5) and order the traces based on their respective average decay rate. Both co-doped NC ensembles show striking similarities with the intrinsic Si NC system, which seems to indicate identical NC qualities. Surprisingly, PL quantum yield values of co-doped NC ensembles are typically much lower than those reported for intrinsic NCs[11,32] (a feature that we also observe from the relative PL intensities in Figure 1g). This leads us to believe that significant carrier quenching for the co-doped ensembles is occurring beyond the resolution of our IA setup (≈200-300 fs), for reasons that are at the moment unclear to us. We can therefore only make statements regarding a subset of the doped NCs (the ones electronically active after 200-300 fs), with the proportion of this subset potentially being determined by the synthesis technique. Along the same lines, the singly P- and B-doped NCs could exhibit similar fast quenching channels invisible to our experimental setup as well. In addition, and in contrast to the co-doped structures, they do show distinctively faster carrier dynamics on the sub 2 ns time-scale in relation to the intrinsic NCs, in line with the lower relative PL intensities (Figure 1g). We speculate that the faster decay dynamics arise from deep defect levels at surface-oxide located- or interstitial-impurity sites[24,25,29] that are potentially related to the specific production method. The greater extent of this e^--h^+ pair/excited state quench for the B-doped NCs might indicate a more challenging route towards high quality B-doped NCs. Interestingly, simultaneous co-doping of both doping species is apparently extensively different in nature than the singly-doping process since it does not create these

Pursuant to the DOE Public Access Plan, this document represents the authors' peer-reviewed, accepted manuscript. The published version of the article is available from the relevant publisher.

defect states. This could be explained by preferential positioning of the B-P pairs at or in the vicinity of the surface (forming static dipoles), as previously suggested by Ref.[41].

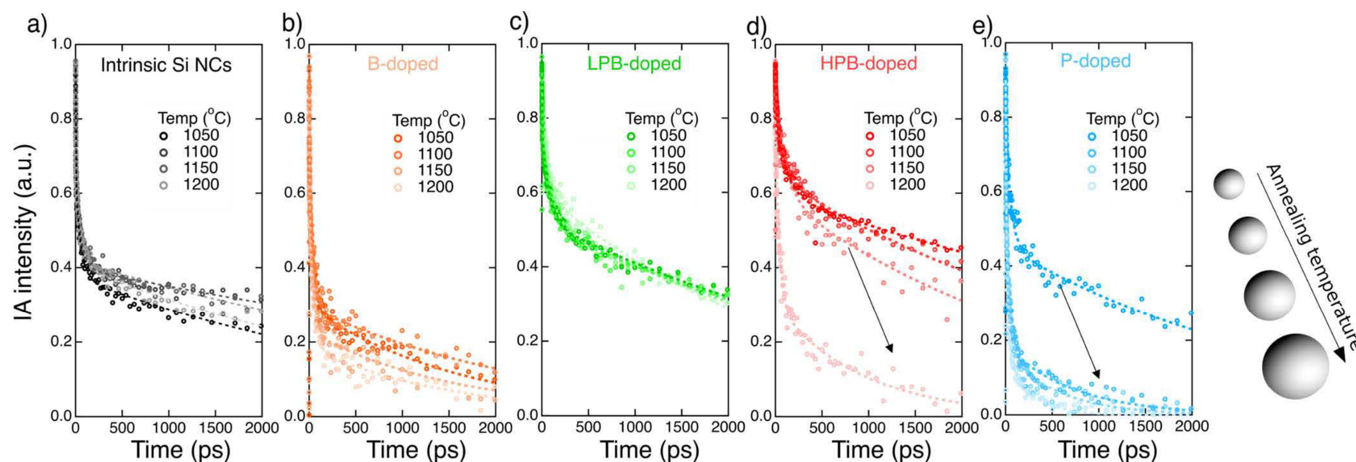

Figure 3. IA traces for all Si NC ensembles, at all annealing temperatures (1050-1200 °C). Traces are displayed for the intrinsic Si NCs (a), B-doped (b), LPB co-doped (c), HPB co-doped (d) and P-doped Si NCs (e). All traces are normalized to 1 at Δt=0. The dashed lines represent triple exponential fits. The black arrows in the panels (d-e) indicate quenched carrier dynamics for higher annealing temperatures.

Figure 3 displays the complete set of IA traces for all samples as the annealing temperature is increased, which is well-known to increase the NC size. Panel (a) shows the growth temperature-independence of the IA traces for the intrinsic Si NC ensembles (gray traces). Apparently, the temperature-induced size variation from 3 to 4 nm does not alter the ultrafast carrier dynamics of the intrinsic NCs. This is indicative for similar quality NC systems. Important to note is that the 10^{-3}-10^{-4} s radiative recombination rate of intrinsic Si NCs does show variation within this size-regime.[32,42] However, the IA time-scale reported here (sub 2 ns) is simply too short to observe such variations in these ultrafast traces. Traces of the B- and LPB-doped NCs show a similar insensitivity to the size change that is induced by the annealing temperature. HPB- and P-doped NC ensembles do however exhibit significantly quenched carrier dynamics upon increasing the annealing temperature (black arrows in Figure 3d, e). Note that we are not aiming to quantify the exact time-scales of the quench since this would require a more fundamental modelling procedure,[23] and is outside of the scope of this work. That said, the trends in carrier dynamics are apparent from the traces in Figure 3. The quench for the HPB-systems (red) starts to kick in at T_{an}=1150 °C and completely takes over at T_{an}=1200 °C. For the P-doped Si NCs all traces at or above T_{an}=1100 °C also exhibit such quenching behavior. Since the IA data for both the intrinsic, B- and LPB-doped Si NC ensembles indicate that the NC quality is insensitive to the annealing temperature, we assume this holds up for the HPB- and P-doped systems as well. As such, the quench with annealing temperature (black arrows) cannot be explained by deterioration of the crystalline structure. This scenario also is

Pursuant to the DOE Public Access Plan, this document represents the authors' peer-reviewed, accepted manuscript. The published version of the article is available from the relevant publisher.

unlikely when one considers that higher temperatures typically create NCs of higher crystalline quality.[43] Therefore, we propose that the observed quench in the HPB- and P-doped Si NC ensembles at high annealing temperature (i.e., larger size) is due to nonradiative trion recombination of the photo-excited e^{-}-h^{+} pairs by electronic interaction with doping-induced free carriers. Upon increasing the annealing temperature (i.e., the NC size), the activation energy (ΔE) is apparently sufficiently minimized to facilitate Coulomb interactions with the free carriers.

<u>Quantification of the NC size-regime</u>

In order to assess the speculated delocalization of the doping-induced carriers, and because PL-based sizing curves are not possible for these doped NC configurations,[28] we developed a NC-sizing method based on the bi-exciton lifetime ($_{bi}$). This metric is known to scale linearly with the NC volume, for both direct and indirect semiconductor nanocrystals,[44] in accordance with the Auger recombination (AR) model.[45] As such, it can be used as a robust sizing method. Figure 4a presents scaled IA traces taken in the multi-excitation regime (i.e., more than one absorbed photon per NC), for the intrinsic Si NC ensembles. Scaling is performed in accordance to the method of Klimov et al.,[45] in which we scaled these multi-excitation traces by subtracting the single-exciton excitation regime traces after normalization (details are given in the Supporting Information – Figure S3). In this way, *n*-exciton lifetimes (with *n* being 2, 3, ... *n*) are given by individual exponential decays. We emphasize that the dynamics in the single-exciton excitation regime are complicated by non-radiative recombination channels, such as trapping (as we showed in Figure 3). This is exactly the reason why we scale the multi-exciton traces to the single-exciton regime before constructing the bi-exciton lifetime. As such, this analysis excludes all non-radiative recombination channels that appear in the single-exciton regime and we are able to focus solely on the Auger recombination of the multiple carriers. Note that this reasoning only holds in the absence of a new class of trap-states that would only be present in the multi-exciton excitation regime. We are not aware of such a scenario. We reconstruct $_{bi}$ (n=2) by applying a single exponential fit to the long tail in Figure 4a (red dashed lines), in line with Ref.[45] – see Figure S6 for a confirmation of this fitting procedure. We plot the resulting $_{bi}$ (ranging from ≈32 – 160 ps) versus the belonging NC volume in Figure 4b to show the expected linear volume-dependence (orange dashed line) of $_{bi}$ for our intrinsic Si NC ensembles. This orange line ($_{bi}$=-28.7 + 4.1· NC_{Volume}) functions as our NC-sizing curve. Next, we measure the $_{bi}$ of all doped NC ensembles (≈20-400 ps) and plot them as a function of their respective annealing temperature (Figure 4c) – all scaled multi-exciton traces from which we construct these lifetimes are presented in Figure S7. As expected, most NC-ensembles show increased $_{bi}$ values upon increasing annealing temperatures (solid disks in Figure 4c), explained by decreased Coulomb interactions for larger sized NCs due to the spatial delocalization.[46] However, some systems (P-doped with T_{an}=1100-1200°C and LPB and HPB at T_{an}=1200°C) exhibit fastened $_{bi}$ values for larger annealing temperatures. These NC systems are represented by the open circles in Figure 4c, and we used the black arrows to indicate shortening of $_{bi}$. Strikingly, apart from LPB T_{an}=1200°C, the exact same NC systems showed the largest deviations in the IA traces in the single-exciton excitation power regime in Figure 3. Based on our prior work where we observed shortening of the $_{bi}$ as a result of an AR process that is fastened by the presence of additional free carriers,[23] this suggests that the photophysics in the present samples are governed by free carrier interactions as well. As such, an increase in

Pursuant to the DOE Public Access Plan, this document represents the authors' peer-reviewed, accepted manuscript. The published version of the article is available from the relevant publisher.

the oscillator strength of the Coulomb-driven process of these free carriers fastens AR. The shortening of the $_{bi}$ therefore directly confirms the speculated delocalization of the doping-induced carriers; by increasing annealing temperatures (i.e., NC sizes), our doped NC systems transition from a localized- to a free-carrier-regime. This facilitates efficient AR (Figure 4c) and quenches the ultrafast carrier dynamics by trion recombination (Figure 3). The direct correlation of both of these effects clarifies the origin of the quench beyond any reasonable doubt and assigns it to nonradiative trion recombination. Interestingly, we do observe free carrier interactions for LPB T_{an}=1200°C through evaluation of $_{bi}$ (Figure 4c), but not in the carrier dynamics in Figure 3. This shows that the free carrier interactions are much more efficiently probed through the quantification of multi-exciton interactions ($_{bi}$). This is expected since the applied scaling method in the multi-excitation regime removes all additional relaxation channels, to arrive at scaled traces that solely depict the multi-exciton interactions. In addition, to verify our findings, we confirmed the delocalization of the doping-induced carriers in Figure S8 by applying a stochastic modelling approach on the multi-exciton dynamics. This method allows to determine the state of the doping-induced carriers without the need for tedious external conductivity measurements (such as the ones used in Refs.[24,25]) or signs of LSPR modes that can only be detected for a large number of free carriers per NC (>10).[47]

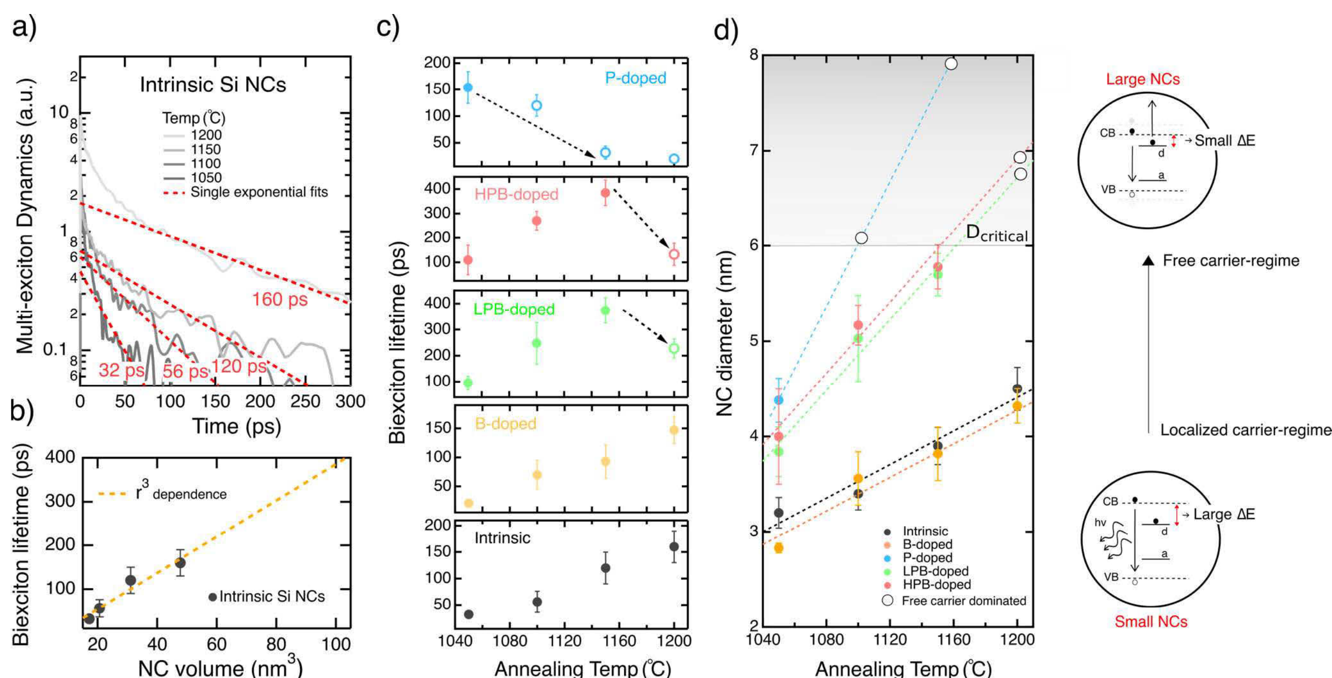

Figure 4. a) Dynamics of multi-excitons, for the intrinsic Si NCs. The traces are scaled following the method of Klimov.[45] The red dashed lines represent single exponential fitting curves, defining the biexciton lifetimes, $_{bi}$. b) $_{bi}$ of the intrinsic Si NCs, as a function of the NC volume (as taken from PL)[33]. The orange linear fit depicts the linear dependence on the NC volume. c) $_{bi}$ as a function of the annealing temperature, for all samples. The black arrows indicate fastening of the $_{bi}$ for increased annealing temperatures. The open circles describe the samples that show fastened carrier dynamics. The disks represent NC systems of which the carrier dynamics are unaffected by doping-induced carriers, including the intrinsic NCs. d) NC diameter as a function of the annealing temperature. For the samples in the localized-carrier-

Pursuant to the DOE Public Access Plan, this document represents the authors' peer-reviewed, accepted manuscript. The published version of the article is available from the relevant publisher.

regime – solid disks – this diameter is based on the $_{bi}$*-*D_{NC} *relation established in Figure 4b for the intrinsic NCs, with the errors determined by the fitting errors of* $_{bi}$*. For the intrinsic NCs, a relative error of 10% is depicted for* D_{NC}*, as estimated from Ref[[33]]. The dashed lines are linear fitting lines/extrapolations and function as guides to the eye. The dashed blue line serves as an indication of the NC size of the P-doped systems based on the LPB- and HPB-systems, see main text for further clarification. The open circles depict the expected diameter for the samples in the free-carrier-regime. The scheme on the right-side illustrates the transition from a localized to a free carrier-regime by changing the NC size.*

We now turn to the quantification of the NC size-regime at which this delocalization occurs. By making use of the $_{bi}$-D_{NC} relation established in Figure 4b for the intrinsic Si NCs, we determine the average diameter of the NC-systems that are in the localized-carrier-regime (solid disks in Figure 4c). Note that we can use this method since the biexciton lifetimes of these doped NCs are unaffected by the doped-induced carriers, in line with Ref.[28]. The solid dots in Figure 4d represent these constructed NC diameters as a function of the annealing temperature (Figure S9 confirms these NC sizes by showing structural analysis through high-resolution transmission electron microscopy, HRTEM). Furthermore, we are aware that the sizes of the NC-ensembles in which the $_{bi}$ is fastened by free carrier interactions (open circles in Figure 4c) cannot be determined through the $_{bi}$-D_{NC} relation. To still get a sense of their average NC size of LPB- and HPB-doped T_{an}=1200°C we extrapolate the linear dependence of the NC diameter on the annealing temperature (as indicated by the dashed lines in Figure 4d). This extrapolation procedure is not possible for the P-doped ensemble since only one sample (T_{an}=1050°C) is in the localized-carrier-regime. Still, based on (1) the knowledge retrieved from the LPB- and HPB-doped samples with free-carrier interactions taking place above a NC size of 6 nm and (2) using Figure 4c that shows free carrier interactions for P-doped NCs at T_{an}>1050°C, we can include the dashed blue line in Figure 4d to exemplify the transition to a free-carrier regime for the P-doped NCs. Hereby we position P-doped T_{an}=1100°C at 6 nm and, as such, provide the under limit of what the P-doped sizes could be. The validity of this size-estimation for the P-doped Si NCs is confirmed by HRTEM images in Figure S9. All of the extrapolation-estimated NC diameters are depicted by the open circles. As expected from the similar PL peak positions in Figure 1f, the B-doped and intrinsic NCs have identical sizes ($D_{NC}\approx$3-4 nm). P-doping and P-B co-doping however facilitates larger NC growth with NCs ranging from $D_{NC}\approx$4-8 nm, depending on the annealing temperature. We ascribe the increase of the size by doping to “softening” of the matrix by P and/or B doping, resulting in larger diffusion lengths of the Si atom. The facilitation of NC growth by the doping incorporation is in line with our TEM size-analysis (Figure S9) and our previous publication on P-B co-doped Si NCs.[28]

Detailed Interpretation

Figure 4d provides us with a critical NC size of $D_{critical}\approx$6 nm at which delocalization of the doping-induced carriers takes place. Note that the intention of this paper is not to define “the” exact critical NC diameter, we are aware that our results do not exhibit enough detail/resolution for such a statement. Our main point is to show that there is “a” critical diameter, and following our data, we propose it is in the vicinity of around 6 nm. The transformation to a free carrier-regime with increased NC sizes can be explained by two

Pursuant to the DOE Public Access Plan, this document represents the authors' peer-reviewed, accepted manuscript. The published version of the article is available from the relevant publisher.

1
2
3
4
5
6
7
8
9
10
11
12
13
14
15
16
17
18
19
20
21
22
23
24
25
26
27
28
29
30
31
32
33
34
35
36
37
38
39
40
41
42
43
44
45
46
47
48
49
50
51
52
53
54
55
56
57
58
59
60

primary scenarios that both affect the energy required to activate the impurities (i.e., the activation energy ΔE).[30] First, as is known for bulk Si, the activation of a donor level depends on its binding energy, which is the energy difference between the conduction (valence) band minimum (maximum) and the donor (acceptor) level. Since quantum confinement blue-shifts the NC bandgap, and the NC size-dependence of the donor/acceptor levels is less prominent,[19] the binding energy is expected to rise as well.[48] This effect is most significant for NC sizes of D_{NC} < 2 nm.[49] Additionally, unscreened Coulomb interactions incited by moving into the nanoscale play a significant role.[50–52] By analysis of the hyperfine structure of electron paramagnetic resonance spectroscopy it is shown that localization of the doping-induced electrons is mainly determined by a reduction of this dielectric screening effect for D_{NC} > 6 nm.[49] Thus, in the intermediate size-regime (2 nm < D_{NC} < 6nm), in which we can find the majority of our NC ensembles, both the dielectric contribution and the quantum confinement-induced bandgap-effect should determine the level of localization of the doping-induced carriers.[30] In this work we probe the end-result of this interplay and the scheme on the right side of Figure 4d depicts the general model. For NC sizes larger than $D_{critical}$, doping produces free majority carriers that alter the photophysics. Si NC samples smaller than $D_{critical}$ can still be substitutional doped, as shown by the donor-acceptor transitions of P-B co-doped Si NCs, but the presence of any doping-induced carriers that remain after incomplete charge compensation will not significantly affect the dynamics of the photo-excited e^{-}-h^{+} pairs. This is promising for photovoltaic applications dealing with these exotic co-doped NCs that are the only Si-based system to date to exhibit optical bandgaps in the range of that for optimal power conversion efficiencies (i.e., ≈0.95 eV).[5] This value is derived upon including the beneficial effect of carrier multiplication (a feature already shown to be facilitated and optimized by close-packed P-B co-doped Si NCs).[14] Our results indicate that this optimal emission energy is already reached in HPB-doped Si NCs with sizes below the critical radius of $D_{critical} \approx 6$ nm (Figure 1f). This indicates that their practical feasibility is not limited by the presence of some remaining free carriers in uncompensated NCs.

Furthermore, with the quantification of $D_{critical}$ we bridge the gap between two recent publications of ours and reflect on several other works as well. In Ref.[28] we reported on a localized doping-induced carrier regime in small (D_{NC} < 6 nm) co-doped NCs, whereas in Ref.[23] we indicated increased Auger recombination rates and negative trion recombination in P-doped Si NCs (D_{NC} > 7 nm). In addition, localized surface plasmon resonance (LSPR) modes – reflecting collective oscillations of free carriers – have only been observed for relatively large Si NCs (D_{NC} >7 nm).[53–55] The model is also in line with hybrid density functional theory calculations for small (2-5 nm) SiO_2-embedded P-doped Si NCs that indicated the incapability of electron donation due to high activation energies.[29] Recent studies of Zacharias et al., showed similar results as well by reporting on the absence of trion recombination in small (D_{NC} < 4 nm) P-doped[25] and B-doped[24] Si NCs in combination with their recent IA-based study on both P- and B-doped NCs.[56] Thus, all these reports fit our findings. An important notion regarding this last B-doped work is that the absence of trion recombination is assigned to the inability of effective doping due to high formation energies of substitutional B-doping sites in small Si NCs (instead of a localization of doping-induced carriers). This could also be the case for our B-doped NCs. As such, we cannot put too much emphasis on the carrier dynamics in the multi-excitation regime (Figure 4c) of these samples since they could simply reflect intrinsic Si NC properties. However,

Pursuant to the DOE Public Access Plan, this document represents the authors' peer-reviewed, accepted manuscript. The published version of the article is available from the relevant publisher.

1 2 3 4 5 6 7 8 9 10 11 12 13 14 15 16 17 18 19 20 21 22 23 24 25 26 27 28 29 30 31 32 33 34 35 36 37 38 39 40 41 42 43 44 45 46 47 48 49 50 51 52 53 54 55 56 57 58 59 60

independently of the doping-state, we can rightfully address the effect of B-impurity incorporation (at the NC surface or in the core) on the NC quality and growth mechanism (Figure 3 and 4d, respectively).

Now we turn to the comparison of our TA data and PL data (Figure 1). In Figure 2a we report on an improved level of surface passivation for the P, LPB and HPB-doped samples. Interestingly, this does not imply an improved PL quantum yield compared to the intrinsic NC ensembles as can be seen in Figure 1. Apart from a surface passivation argument one thus encounters additional nonradiative components such as e.g., interstitial site-induced defects, a lack of complete crystallization that would induce grain-boundary type defects, the presence of nonradiative trion recombinations (as we detailedly discuss in this work) and other types of nonradiative recombination channels that could affect the PL quantum yield. Depending on the time-scales of these scenarios they could be visible through IA spectroscopy or not. In particular, PL quenching effects which are on (1) time-scales faster than the temporary resolution of the setup (≈200-300 fs) and (2) on time-scales longer than >2 ns, are not considered by the TA measurements. Furthermore, the IA dynamics could be selective to certain states over/underestimating the observed results. Hence, it is important to realize that increasing the surface passivation upon doping the NCs is only one of the parameters that is incorporated in the PL quantum yield and it can even coincide with a decreased PL quantum yield, as observed here. Especially the state of the doping-induced carriers is important: we observe PL for all doped NC systems that are in the localized-carrier-regime. PL is as good as prohibited as soon as the doped NC systems become big enough to be dominated by the free-carrier-regime (HPB1200 and P1100-1200). Interestingly, emission from P1050- and all B-doped Si NCs seems to originate from excitonic band-to-band transitions, as can be deduced from the correlation between the PL peak position (Figure 1f) and the estimated NC diameter (Figure 4d) for intrinsic NCs, following Ref.[[33]]. This is in contrast to the optically active donor-acceptor transitions of the P-B co-doped NC ensembles which are in the localized carrier regime (LPB1050-1150 and HPB1050-1150).[18,34] A quantitative comparison between the IA and PL measurements is given in Figure S11. In conclusion, and in relation to the present literature, we thus argue that the PL quantum yield behavior of doped Si NCs, and P-B co-doped NCs (as presented in Ref.[34]) in particular, should reflect mutually connected processes, such as: 1) increased surface interactions for excitons in small NCs,[57] 2) higher defect probability for larger NCs (due to a statistical argument dealing with larger NC surfaces),[32] 3) the mobility-state of the doped carrier regime and 4) potential doping-induced defect states, with the latter two points being quantitatively addressed for the first time in this work.

Conclusions

To summarize, we extend our ultrafast spectroscopy work on the electronic interactions of doping-induced carriers in Si NCs. In this effort we dope Si NCs of various diameters with n-, p- and np-type configurations and hereby control the delocalization of the doping-induced carriers. We define a critical NC size ($D_{critical} \approx 6$ nm) at which the activation energy (ΔE) becomes small enough to create free majority carriers. Lifetimes of photo-exited e^--h^+ pairs for larger NCs ($D_{NC} > D_{critical}$) are significantly shortened due to strong nonradiative trion recombinations with free carriers. These Coulomb interactions with the free carriers also fasten

Pursuant to the DOE Public Access Plan, this document represents the authors' peer-reviewed, accepted manuscript. The published version of the article is available from the relevant publisher.

1
2
3
4
5
6
7
8
9
10
11
12
13
14
15
16
17
18
19
20
21
22
23
24
25
26
27
28
29
30
31
32
33
34
35
36
37
38
39
40
41
42
43
44
45
46
47
48
49
50
51
52
53
54
55
56
57
58
59
60

the AR process of multiple excited e^--h^+ pairs in large NCs. Moreover, our results strongly suggest preferential paired positions of the dopants upon simultaneous co-doping with the n- and p-type doping species, in line with a surface-located static dipole model of the dopant pairs. These results, combined with the obtained insights in the NC growth and passivation mechanics, could guide applied research directions dealing with doped Si NC systems. The take-home message depends on the practical applicability of the device in mind. Charge transfer-based systems should aim for delocalization of the doping-induced carriers ($D_{NC} > D_{critical}$). Other systems relying on long carrier lifetimes and high PL activities can only be facilitated through NC systems in the localized-carrier-regime ($D_{NC} < D_{critical}$).

Associated Content

Supporting Information

The supporting information is available free of charge on the ACS Publications website at DOI:…

> 1) X-ray photoelectron spectroscopy, 2) Linear absorption spectra, 3) multi-exciton excitation regime of the induced absorption (IA) traces, 4) Surface quality by IA, 5) Details of Intrinsic Si NC IA traces, in the linear excitation regime, 6) Multi-exciton recombination with n-number of excitons, 7) Deduction of the biexciton lifetimes of all doped NC structures, 8) Modeling the Auger recombination process by symmetric interactions, 9) Verification of the NC sizes by high-resolution transmission microscopy (HRTEM), 10) NIR probing independence of the carrier dynamics, 11) Excitation density and the average number of absorbed photons in the single-exciton excitation regime, 12) Comparison between the PL and IA datasets.

Author Contributions

R.L conceived the project, conducted the experiments, analyzed and interpreted the data and wrote the manuscript. H.S produced the sputtered the NC films, assisted in the data interpretations and co-wrote the manuscript. N. R. N assisted in the data interpretations and co-wrote the manuscript. M.F. facilitated the sample production, assisted in the data interpretations and co-wrote the manuscript.

Acknowledgements

R.L. and N.R.N. are employees of the Alliance for Sustainable Energy, LLC, the manager and operator of the National Renewable Energy Laboratory for the U.S. Department of Energy (DOE) under Contract No. DE-AC36-08GO28308. R.L. was funded under the National Renewable Energy Laboratory (NREL) LDRD program, Nozik Director's Postdoctoral Fellowship. N.R.N. was funded by the U.S. Department of Energy, Office of Science, Office of Basic Energy Sciences, Division of Chemical Sciences, Geosciences, and Biosciences, Solar Photochemistry Program. The views expressed in the article do not necessarily represent the views of the DOE or the U.S. Government. The U.S. Government retains and the publisher, by accepting the article for publication, acknowledges that the U.S. Government retains a nonexclusive, paid-up, irrevocable, worldwide license to publish or reproduce the published form of this work, or allow others to do so, for U.S. Government purposes. M.F acknowledges the 2015 JST Visegrad Group

Pursuant to the DOE Public Access Plan, this document represents the authors' peer-reviewed, accepted manuscript. The published version of the article is available from the relevant publisher.

1
2
3
4
5
6
7
8
9
10
11
12
13
14
15
16
17
18
19
20
21
22
23
24
25
26
27
28
29
30
31
32
33
34
35
36
37
38
39
40
41
42
43
44
45
46
47
48
49
50
51
52
53
54
55
56
57
58
59
60

(V4)–Japan Joint Research Project on Advanced Materials and JSPS KAKENHI Grant No. 16H03828. H.S acknowledges JSPS KAKENHI Grant No. 18K14092.

References

(1) Trinh, M. T.; Limpens, R.; De Boer, W. D. A. M.; Schins, J. M.; Siebbeles, L. D. A.; Gregorkiewicz, T. Direct Generation of Multiple Excitons in Adjacent Silicon Nanocrystals Revealed by Induced Absorption. *Nat. Photonics* **2012**, *6*, 316–321.

(2) Bruhn, B.; Limpens, R.; Chung, N. X.; Schall, P.; Gregorkiewicz, T. Spectroscopy of Carrier Multiplication in Nanocrystals. **2016**, 6, 20538.

(3) Beard, M. C.; Knutsen, K. P.; Yu, P.; Luther, J. M.; Song, Q.; Metzger, W. K.; Ellingson, R. J.; Nozik, A. J. Multiple Exciton Generation in Colloidal Silicon Nanocrystals. *Nano Lett.* **2007**, *7*, 2506–2512..

(4) Shockley, W.; Queisser, H.; Queisser, H. J. The Shockley-Queisser Limit. *J. Appl. Phys.* **1961**, *32*, 510–519.

(5) Nozik, A. J. Nanoscience and Nanostructures for Photovoltaics and Solar Fuels. *Nano Lett.* **2010**, *10*, 2735–2741

(6) Wheeler, L. M.; Nichols, A. W.; Chernomordik, B. D.; Anderson, N. C.; Beard, M. C.; Neale, N. R. All-Inorganic Germanium Nanocrystal Films by Cationic Ligand Exchange. *Nano Lett.* **2016,** 16, 1949-195

(7) Luther, J. M.; Law, M.; Beard, M. C.; Song, Q.; Reese, M. O.; Ellingson, R. J.; Nozik, A. J. Schottky Solar Cells Based on Colloidal Nanocrystal Films. *Nano Lett.* **2008**, *8*, 3488–3492.

(8) Lee, J. S.; Kovalenko, M. V.; Huang, J.; Chung, D. S.; Talapin, D. V. Band-like Transport, High Electron Mobility and High Photoconductivity in All-Inorganic Nanocrystal Arrays. *Nat. Nanotechnol.* **2011**, *6*, 348–352.

(9) Semonin, O. E.; Luther, J. M.; Choi, S.; Chen, H.-Y.; Gao, J.; Nozik, A. J.; Beard, M. C. Peak External Photocurrent Quantum Efficiency Exceeding 100% via MEG in a Quantum Dot Solar Cell. *Science.* **2011**, *334*, 1530–1533.

(10) Holman, Z. C.; Liu, C. Y.; Kortshagen, U. R. Germanium and Silicon Nanocrystal Thin-Film Field-Effect Transistors from Solution. *Nano Lett.* **2010**, *10*, 2661–2666.

(11) Sugimoto, H.; Fujii, M.; Imakita, K.; Hayashi, S.; Akamatsu, K. Codoping N-and P-Type Impurities in Colloidal Silicon Nanocrystals-Controlling Luminescence Energy from below Bulk Band Gap to Visible Range. *J. Phys. Chem. C* **2013**, *117*, 11850–11857.

(12) Almeida, A. J.; Sugimoto, H.; Fujii, M.; Brandt, M. S.; Stutzmann, M.; Pereira, R. N. Doping Efficiency and Confinement of Donors in Embedded and Free Standing Si Nanocrystals. *Phys. Rev. B* **2016**, *93*, 1–9.

(13) Sugimoto, H.; Fujii, M.; Imakita, K. Synthesis of Boron and Phosphorus Codoped All-Inorganic Colloidal Silicon Nanocrystals from Hydrogen Silsesquioxane. **2014**, 6, 12354-12359.

(14) Xuan Chung, N.; Limpens, R.; de Weerd, C.; Lesage, A.; Fujii, M.; Gregorkiewicz, T. Towards Practical Carrier Multiplication: Donor/acceptor Co-Doped Si Nanocrystals in SiO2. *ACS Photonics* **2018**, DOI: 10.1021/acsphotonics.8b00144.

(15) Das, P.; Jana, N. R. Highly Colloidally Stable Hyperbranched Polyglycerol Grafted Red Fluorescent Silicon Nanoparticle as Bioimaging Probe. *ACS Appl. Mater. Interfaces* **2014**,

Pursuant to the DOE Public Access Plan, this document represents the authors' peer-reviewed, accepted manuscript. The published version of the article is available from the relevant publisher.

6, 4301–4309.
(16) Somogyi, B.; Derian, R.; Štich, I.; Gali, A. High-Throughput Study of Compositions and Optical Properties in Heavily Co-Doped Silicon Nanoparticles. *J. Phys. Chem. C* **2017**, 121, 27741-27750.
(17) Ni, Z.; Ma, L.; Du, S.; Xu, Y.; Yuan, M.; Fang, H.; Wang, Z.; Xu, M.; Li, D.; Yang, J.; et al. Plasmonic Silicon Quantum Dots Enabled High-Sensitivity Ultrabroadband Photodetection of Graphene-Based Hybrid Phototransistors. *ACS Nano* **2017**, *11*, 9854–9862.
(18) Ashkenazi, O.; Azulay, D.; Balberg, I.; Kano, S.; Sugimoto, H.; Fujii, M.; Millo, O. Size-Dependent Donor and Acceptor States in Codoped Si Nanocrystals Studied by Scanning Tunneling Spectroscopy. *Nanoscale* **2017**, *9*, 17884–17892.
(19) Hori, Y.; Kano, S.; Sugimoto, H.; Imakita, K.; Fujii, M. Size-Dependence of Acceptor and Donor Levels of Boron and Phosphorus Codoped Colloidal Silicon Nanocrystals. *Nano Lett.* **2016**, *16*, 2615–2620.
(20) Li, D.; Jiang, Y.; Liu, J.; Zhang, P.; Xu, J.; Li, W.; Chen, K. Modulation of Surface States by Phosphorus to Improve the Optical Properties of Ultra-Small Si Nanocrystals. *Nanotechnology* **2017**, *28*.
(21) Mimura, A.; Fujii, M.; Hayashi, S.; Kovalev, D.; Koch, F. Photoluminescence and Free-Electron Absorption in Heavily Phosphorus-Doped Si Nanocrystals. *Phys. Rev. B - Condens. Matter Mater. Phys.* **2000**, *62*, 12625–12627.
(22) Frégnaux, M.; Khelifi, R.; Muller, D.; Mathiot, D. Optical Characterizations of Doped Silicon Nanocrystals Grown by Co-Implantation of Si and Dopants in SiO2. *J. Appl. Phys.* **2014**, *116*.
(23) Limpens, R.; Neale, N. R. Free Electron-Driven Photophysics in N-Type Doped Silicon Nanocrystals. *Nanoscale.* **2018,** DOI: 10.1039/C8NR02173B.
(24) Hiller, D.; López-Vidrier, J.; Gutsch, S.; Zacharias, M.; Wahl, M.; Bock, W.; Brodyanski, A.; Kopnarski, M.; Nomoto, K.; Valenta, J.; et al. Boron-Incorporating Silicon Nanocrystals Embedded in SiO2: Absence of Free Carriers vs. B-Induced Defects. *Sci. Rep.* **2017**, *7*.
(25) Hiller, D.; López-Vidrier, J.; Gutsch, S.; Zacharias, M.; Nomoto, K.; König, D. Defect-Induced Luminescence Quenching vs. Charge Carrier Generation of Phosphorus Incorporated in Silicon Nanocrystals as Function of Size. *Sci. Rep.* **2017**, *7*, 1–12.
(26) Lu, P.; Mu, W.; Xu, J.; Zhang, X.; Zhang, W.; Li, W.; Xu, L.; Chen, K. Phosphorus Doping in Si nanocrystals/SiO 2 Msultilayers and Light Emission with Wavelength Compatible for Optical Telecommunication. *Sci. Rep.* **2016**, *6*, 1–12.
(27) Kachurin, G. A.; Cherkova, S. G.; Volodin, V. A.; Kesler, V. G.; Gutakovsky, A. K.; Cherkov, A. G.; Bublikov, A. V.; Tetelbaum, D. I. Implantation of P Ions in SiO2layers with Embedded Si Nanocrystals. *Nucl. Instruments Methods Phys. Res. Sect. B Beam Interact. with Mater. Atoms* **2004**, *222*, 497–504.
(28) Limpens, R.; Fujii, M.; Neale, N. R.; Gregorkiewicz, T. Negligible Electronic Interaction between Photoexcited Electron-Hole Pairs and Free Electrons in Phosphorus-Boron Co-Doped Silicon Nanocrystals. *J. Phys. Chem. C* **2018**, *122*, 6397-6404.
(29) König, D.; Gutsch, S.; Gnaser, H.; Wahl, M.; Kopnarski, M.; Göttlicher, J.; Steininger, R.; Zacharias, M.; Hiller, D. Location and Electronic Nature of Phosphorus in the Si Nanocrystal - SiO2 System. *Sci. Rep.* **2015**, *5*.

Pursuant to the DOE Public Access Plan, this document represents the authors' peer-reviewed, accepted manuscript. The published version of the article is available from the relevant publisher.

(30) Marri, I.; Degoli, E.; Ossicini, S. Doped and Codoped Silicon Nanocrystals: The Role of Surfaces and Interfaces. *Prog. Surf. Sci.* **2017**.

(31) Fujii, M.; Sugimoto, H.; Imakita, K. All-Inorganic Colloidal Silicon Nanocrystals—surface Modification by Boron and Phosphorus Co-Doping. *Nanotechnology* **2016**, *27*, 262001.

(32) Limpens, R.; Luxembourg, S. L.; Weeber, A. W.; Gregorkiewicz, T. Emission Efficiency Limit of Si Nanocrystals. *Nat. Publ. Gr.* **2016**, 6, 19566.

(33) Takeoka, S.; Fujii, M.; Hayashi, S. Size-Dependent Photoluminescence from Surface-Oxidized Si Nanocrystals in a Weak Confinement Regime. *Phys. Rev. B - Condens. Matter Mater. Phys.* **2000**, *62*, 16820–16825.

(34) Sugimoto, H.; Fujii, M.; Imakita, K.; Hayashi, S.; Akamatsu, K. Phosphorus and Boron Codoped Colloidal Silicon Nanocrystals with Inorganic Atomic Ligands. *J. Phys. Chem. C* **2013**, *117*, 6807–6813.

(35) Fujii, M.; Yamaguchi, Y.; Takase, Y.; Ninomiya, K.; Hayashi, S. Control of Photoluminescence Properties of Si Nanocrystals by Simultaneously Doping N- and P-Type Impurities. *Appl. Phys. Lett.* **2004**, *85*, 1158–1160.

(36) Trinh, M. T.; Limpens, R.; Gregorkiewicz, T. Experimental Investigations and Modeling of Auger Recombination in Silicon Nanocrystals. *J. Phys. Chem. C* **2013**, 117, 5963-5968.

(37) Limpens, R.; Gregorkiewicz, T. Spectroscopic Investigations of Dark Si Nanocrystals in SiO2 and Their Role in External Quantum Efficiency Quenching. *J. Appl. Phys.* **2013**, *114*, 074304.

(38) Stegner, A. R.; Pereira, R. N.; Lechner, R.; Klein, K.; Wiggers, H.; Stutzmann, M.; Brandt, M. S. Doping Efficiency in Freestanding Silicon Nanocrystals from the Gas Phase: Phosphorus Incorporation and Defect-Induced Compensation. *Phys. Rev. B - Condens. Matter Mater. Phys.* **2009**, *80*, 1–10.

(39) Puthen Veettil, B.; Wu, L.; Jia, X.; Lin, Z.; Zhang, T.; Yang, T.; Johnson, C.; McCamey, D.; Conibeer, G.; Perez-Würfl, I. Passivation Effects in B Doped Self-Assembled Si Nanocrystals. *Appl. Phys. Lett.* **2014**, *105*.

(40) Nomoto, K.; Sugimoto, H.; Breen, A.; Ceguerra, A. V.; Kanno, T.; Ringer, S. P.; Wurfl, I. P.; Conibeer, G.; Fujii, M. Atom Probe Tomography Analysis of Boron And/or Phosphorus Distribution in Doped Silicon Nanocrystals. *J. Phys. Chem. C* **2016**, *120*, 17845–17852.

(41) Guerra, R.; Ossicini, S. Preferential Positioning of Dopants and Co-Dopants in Embedded and Freestanding Si Nanocrystals. *J. Am. Chem. Soc.* **2014**, *136*, 4404–4409.

(42) Miura, S.; Nakamura, T.; Fujii, M.; Inui, M.; Hayashi, S. Size Dependence of Photoluminescence Quantum Efficiency of Si Nanocrystals. *Phys. Rev. B* **2006**, *73*, 245333.

(43) Iacona, F.; Bongiorno, C.; Spinella, C.; Boninelli, S.; Priolo, F. Formation and Evolution of Luminescent Si Nanoclusters Produced by Thermal Annealing of SiOx Films. *J. Appl. Phys.* **2004**, *95*, 3723–3732.

(44) Robel, I.; Gresback, R.; Kortshagen, U.; Schaller, R. D.; Klimov, V. I. Universal Size-Dependent Trend in Auger Recombination in Direct-Gap and Indirect-Gap Semiconductor Nanocrystals. *Phys. Rev. Lett.* **2009**, *102*, 1–4.

(45) Klimov, V. I.; Mikhailovsky, A. A.; McBranch, D. W.; Leatherdale, C. A.; Bawendi, M. G. Quantization of Multiparticle Auger Rates in Semiconductor Quantum Dots. *Science.* **2000**, *287*, 1011–1014.

Pursuant to the DOE Public Access Plan, this document represents the authors' peer-reviewed, accepted manuscript. The published version of the article is available from the relevant publisher.

(46) Beard, M. C.; Johnson, J. C.; Luther, J. M.; Nozik, A. J. Multiple Exciton Generation in Quantum Dots versus Singlet Fission in Molecular Chromophores for Solar Photon Conversion. *Philos. Trans. R. Soc. A Math. Phys. Eng. Sci.* **2015**, *373*, 20140412–20140412.

(47) Luther, J. M.; Jain, P. K.; Ewers, T.; Alivisatos, A. P. Localized Surface Plasmon Resonances Arising from Free Carriers in Doped Quantum Dots. *Nat. Mater.* **2011**, *10*, 361–366.

(48) Xu, Q.; Luo, J. W.; Li, S. S.; Xia, J. B.; Li, J.; Wei, S. H. Chemical Trends of Defect Formation in Si Quantum Dots: The Case of Group-III and Group-V Dopants. *Phys. Rev. B - Condens. Matter Mater. Phys.* **2007**, *75*, 1–6.

(49) Pereira, R. N.; Stegner, A. R.; Andlauer, T.; Klein, K.; Wiggers, H.; Brandt, M. S.; Stutzmann, M. Dielectric Screening versus Quantum Confinement of Phosphorus Donors in Silicon Nanocrystals Investigated by Magnetic Resonance. *Phys. Rev. B - Condens. Matter Mater. Phys.* **2009**, *79*.

(50) Cantele, G.; Degoli, E.; Luppi, E.; Magri, R.; Ninno, D.; Iadonisi, G.; Ossicini, S. First-Principles Study of N- and P-Doped Silicon Nanoclusters. *Phys. Rev. B - Condens. Matter Mater. Phys.* **2005**, *72*, 2–5.

(51) Melnikov, D. V.; Chelikowsky, J. R. Quantum Confinement in Phosphorus-Doped Silicon Nanocrystals. *Phys. Rev. Lett.* **2004**, *92*, 4.

(52) Ögüt, S.; Chelikowsky, J. R.; Louie, S. G. Quantum Confinement and Optical Gaps in Si Nanocrystals. *Phys. Rev. Lett.* **1997**, *79*, 1770–1773.

(53) Diroll, B. T.; Schramke, K. S.; Guo, P.; Kortshagen, U. R.; Schaller, R. D. Ultrafast Silicon Photonics with Visible to Mid-Infrared Pumping of Silicon Nanocrystals. *Nano Lett.* **2017**, *17*, 6409–6414.

(54) Rowe, D. J.; Jeong, J. S.; Mkhoyan, K. A.; Kortshagen, U. R. Phosphorus-Doped Silicon Nanocrystals Exhibiting Mid-Infrared Localized Surface Plasmon Resonance - Supplementary Information. *Nano Lett.* **2013**, Supplementary Information.

(55) Zhang, H.; Zhang, R.; Schramke, K. S.; Bedford, N. M.; Hunter, K.; Kortshagen, U. R.; Nordlander, P. Doped Silicon Nanocrystal Plasmonics. *ACS Photonics* **2017**, *4*, 963–970.

(56) Hiller, D.; López-Vidrier, J.; Nomoto, K.; Wahl, M.; Bock, W.; Chlouba, T.; Trojánek, F.; Gutsch, S.; Zacharias, M.; König, D.; et al. Absence of Free Carriers in Silicon Nanocrystals Grown from Phosphorus- and Boron-Doped Silicon-Rich Oxide and Oxynitride. *Beilstein J. Nanotechnol.* **2018**, *9*, 1501–1511.

(57) Yu, Y.; Fan, G.; Fermi, A.; Mazzaro, R.; Morandi, V.; Ceroni, P.; Smilgies, D.-M.; Korgel, B. A. Size-Dependent Photoluminescence Efficiency of Silicon Nanocrystal Quantum Dots. *J. Phys. Chem. C* **2017**, 121, 23240-23248.

Pursuant to the DOE Public Access Plan, this document represents the authors' peer-reviewed, accepted manuscript. The published version of the article is available from the relevant publisher.

1
2
3
4
5
6
7
8
9
10
11
12
13
14
15
16
17
18
19
20
21
22
23
24
25
26
27
28
29
30
31
32
33
34
35
36
37
38
39
40
41
42
43
44
45
46
47
48
49
50
51
52
53
54
55
56
57
58
59
60

For Table of Contents Use Only

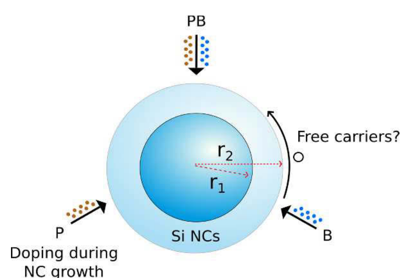

Manuscript title: Critical size for carrier delocalization in doped silicon nanocrystals: a study by ultrafast spectroscopy

Name of Authors: Rens Limpens, Hiroshi Sugimoto, Nathan R. Neale & Minoru Fujii

Brief Synopsis: By ultrafast spectroscopy we show that there exists a critical NC size below which doping-induced carriers behave as localized carriers. These results indicate that the practical photovoltaic feasibility of co-doped Si NCs is not limited by the presence of some remaining free carriers in uncompensated NCs.

Pursuant to the DOE Public Access Plan, this document represents the authors' peer-reviewed, accepted manuscript. The published version of the article is available from the relevant publisher.